Journal of JSEM, Vol.10, Special Issue (2010) 210-214

Formation of Nanoporous Anodic Oxide Films on Ti-Al Microchannel Walls

Masashi ISHIDA[1], Tatsuya OHMI[1], Masatoshi SAKAIRI[1] and Manabu IGUCHI[1]

[1]Division of Materials Science and Engineering, Graduate School of Engineering, Hokkaido University, Sapporo 060-8628, Japan

(*Received 31 January 2010; received in revised form 18 May 2010; accepted 12 June 2010*)

Abstract

Fabrication of a nanoporous anodic oxide film on the inner wall of a microchannel was experimented. The microchannel was produced in a titanium body by a powder-metallurgical microchanneling process and was lined with a Ti-Al alloy layer. We found an appropriate anodic condition for an exposed planner surface of the Ti-Al alloy layer. In the case of the microchannel, the growth of the nanoporous oxide film tended to retard deep inside the channel. This problem was easily solved by lengthening the anodic oxidation time.

Key words

Microchannel, Powder Metallurgy, Infiltration, Anodic Oxidation, Titanium-Aluminum Alloy

1. Introduction

Nowadays, there are a lot of environmental problems such as acid rain, ozone depletion, global heating, urban NOx, the environmental burden of waste products treatment and so on. With these problems as a background, metallic microreactors for high-temperature catalytic reactions are attracting attention. The high specific surface area due to the microchannel structure with a characteristic length from several to several hundreds μm and the high heat conductivity of the metallic material permit high efficiency of the catalytic reaction and the precise temperature control.

However, in the conventional microchanneling methods such as precision machining and photoetching, complicated and exact work is necessary to form three-dimensional microchannel networks. Thus, the processing time and cost increase remarkably.

Some of the authors investigated a powder-metallurgical microchanneling process to reduce the process steps and the manufacturing cost.[1-4] In our experiments, a titanium powder compact containing aluminum wire was sintered at temperatures between the melting points of aluminum and titanium. Figure 1 shows a Ti-Al binary alloy phase diagram [5]. The melting point of titanium is 1010 K higher than that of aluminum.

During sintering, molten aluminum migrates to the titanium powder region by infiltration and/or diffusion, and then a long cavity, or the microchannel, is produced. A Ti-Al alloy layer lining the microchannel is also produced simultaneously. In this process, the titanium powder compact makes the body of the device and the aluminum wire gives the configuration of the microchannel. We call the former metal the body metal and latter metal the sacrificial-core metal. We found that many kinds of combinations of the metals make the microchannel structure by such a simple and economical process.

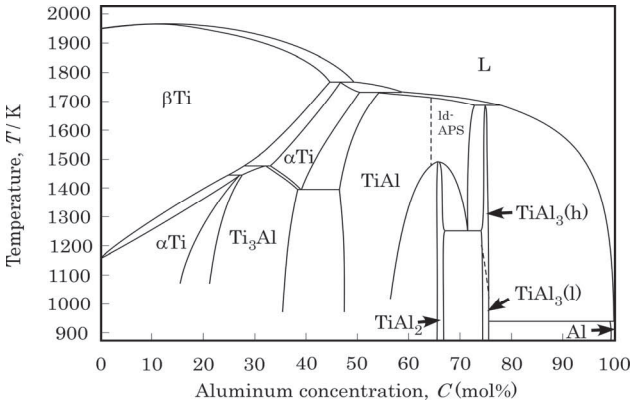

Fig. 1 A Ti-Al binary alloy phase diagram based on the report by Schuster and Palm [5]

In the present study, we focused on the formation of nanoporous oxide films by anodic oxidation of titanium and Ti-Al alloys. The oxide films with nanoporous structure have large specific surface area and high heat and corrosion resistance. If such a nanoporous oxide film can be produced on the inner wall of the microchannel, it must be suitable for a catalyst support for high-temperature catalytic reactions. Backward et al. succeeded to produce such a nanoporous oxide film on the surfaces of titanium and TiAl plates by anodic oxidation.[6] For the anodic oxidation of titanium, the following reactions were reported.

$$\mathrm{Ti} + 2\mathrm{H_2O} \rightarrow \mathrm{TiO_2} + 4\mathrm{H^+} + 4\mathrm{e^-} \quad (1)$$

$$\mathrm{TiO_2} + 4\mathrm{H^+} + 6\mathrm{F^-} \rightarrow \left[\mathrm{TiF_6}\right]^{2-} + 2\mathrm{H_2O} \quad (2)$$

First, a titanium oxide film is formed by the reaction (1), and then, dissolution of the oxide occurs in random order by the reaction (2). In the next stage, local dissolution sites grow up, and the nanoporous oxide film is formed. The diameter and depth of the nanopore can be controlled by the condition of anodic oxidation (solution composition, voltage and time).[6-11] In the present study, anodic oxidation was experimented on the Ti-Al lining layers, which are not always homogeneous in composition and often have hubbly surface.

2. Experimental Procedure

2.1 Anodic oxidation of planar lining layers

The Ti-Al alloy lining layers are produced by reactive infiltration of molten aluminum into the titanium powder region, and therefore their composition, structure and asperity of the surface are changed depending on the sintering conditions.[4] As a first step, therefore, anodic

oxidation of planar lining layers was conducted in order to find the optimum condition for producing the nanoporous oxide film. Titanium powder with average particle size of 45 μm was used as the body metal powder, and an aluminum disk 19 mm in diameter and 100 μm in thickness was used as the sacrificial core. A body metal powder containing a sacrificial-core disc was uniaxially compressed under 530 MPa at room temperature. The shape of the resulted compact specimen was a columnar 20 mm in diameter and 5 mm in height as shown in Fig. 2(a). The compact specimen was heated at a constant rate of 0.2 K/s from room temperature to 1273 K or 1473 K and then furnace cooled at 0.4 K/s. The planar lining layers which were produced on the inner wall of the disk-like cavity were exposed by separating the sintered specimen into two parts as shown in Fig. 2(b). The surface of the lining layer was anodized at room temperature at 20 V. The anodic oxidation time, τ_a, was 3.6 ks. Titanium plate was used as the cathode and 1 kmol/m^3 H_2SO_4 with 0.05, 0.10 or 0.15wt% HF were used as the solution [6]. The surface and cross-section structures of the specimens before and after anodic oxidation were observed by using back-scattered electron images of SEM and FE-SEM (JEOL JSM-6500F). Element analysis was performed using EPMA (JEOL JXA-8900M). For comparison, sintered titanium specimens with no sacrificial core were also anodized in the same conditions.

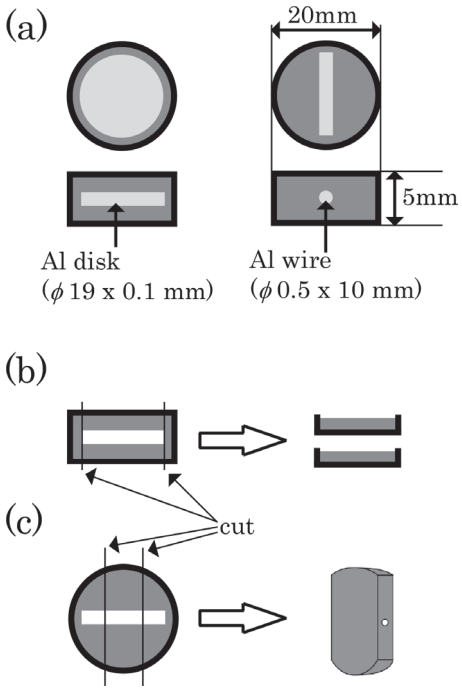

Fig. 2 Preparation of the specimens. (a) The compact specimens. (b) Method to prepare the specimen for anodic oxidation of the exposed planar lining layer. (c) Method to prepare the specimen for anodic oxidation of the inner wall of the microchannel

2.2 Anodic oxidation of the inner wall of the microchannel

The microchannel was produced using the aluminum wire with the diameter of 500 μm as the sacrificial core. The specimen after sintering was cut to thickness of 5 mm. The microchannel penetrated the specimen in the thickness direction (see Fig. 2(c)).

The size of the compact specimen, the compacting pressure, the heat-treatment condition and the anodizing condition were same as the case of the planar sacrificial core. In addition, the cases when τ_a = 7.2 ks and 10.8 ks were also examined.

3. Results

3.1 Structure and composition of the planar lining layer

Figure 3 shows the SEM image of the surface of the inner wall of the disk-like cavity produced by using an aluminum disk as the sacrificial core. Results of point measurements by EPMA are also presented in Fig. 3. Maximum temperature during sintering was 1273 K. There were lots of microscopic asperities on the surface. The compositions measured on the inner-wall surface were within the composition range of Ti_3Al intermetallic compound. The alloyed surface was produced by the reaction between the molten aluminum and the titanium powder.

Figures 4(a) and (b) show a cross-sectional structure near the inner wall shown in Fig. 3, and the concentration profiles measured along the line AB, respectively. The thickness of the lining layer was 300 μm. Composition of the lining layer was inhomogeneous, and Ti_3Al and Ti solid solution were detected. This result shows that aluminum had not diffused completely inside the titanium powder particles.

Figures 5 and 6 show the results in the case when the maximum temperature was 1473 K. Figure 5 shows the structure of the surface of the inner wall of the cavity and the results of the composition analysis. The irregularity of the surface is similar to Fig. 3. On the other hand, the composition profile illustrated in Fig. 6(b) shows a gradual composition change across the lining layer and no vestige of the titanium powder particles. According to the Ti-Al phase diagram in Fig. 1, the composition at the surface of the lining layer (approximately Ti-17mol%Al) corresponds to the coexistence zone of α-Ti solid solution and Ti_3Al at room temperature, but the β-Ti solid solution area at 1473 K. Judging from the smooth concentration profiles in Fig. 6(b), the main constituent phase is probably α- or β-Ti solid solution. There also is a possibility that very fine intermetallic compounds had been precipitated from the supersaturated solid solution.

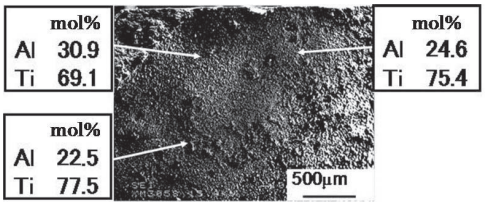

Fig. 3 SEM image of the inner wall of the cavity produced in the specimen heat-treated at 1273 K and the results of EPMA point analysis

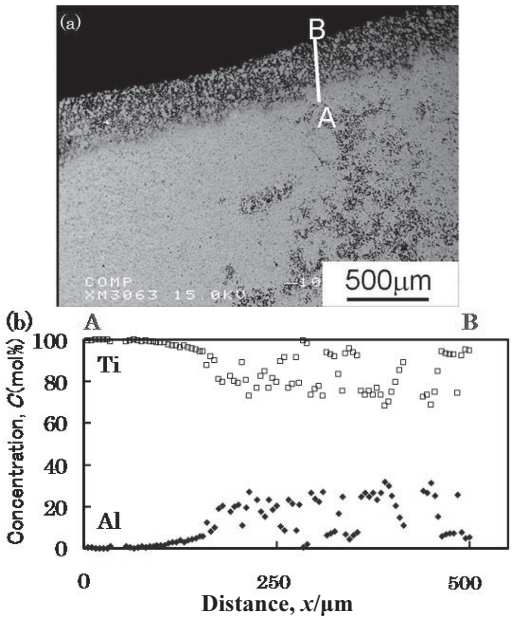

Fig. 4 Structure of the lining layer produced in the specimen heat-treated at 1273 K (a), and the concentration profiles (b), which were measured along the line AB shown in (a)

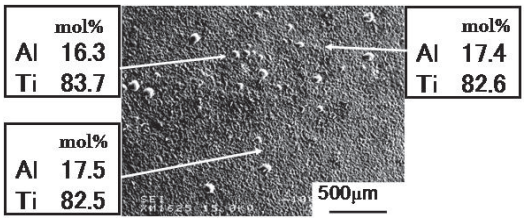

Fig. 5 SEM image of the void surface of the specimen heat-treated at 1473 K and the results of EPMA point analysis

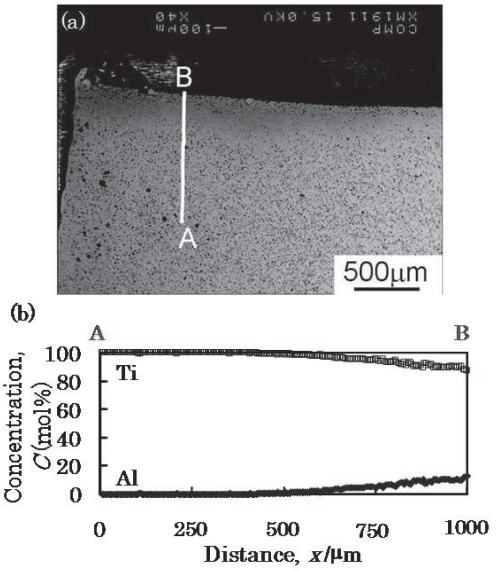

Fig. 6 Structure of the lining layer produced in the specimen heat-treated at 1473 K (a), and the concentration profiles (b), which were measured along the line AB shown in (a)

3.2 Anodic oxidation of the surface of the planar lining layer

Figure 7 depicts the results of the anodic oxidation experiments for the planar lining layers produced at 1273 K and 1473 K. Results of the comparative experiments using the sintered titanium compacts are also shown.

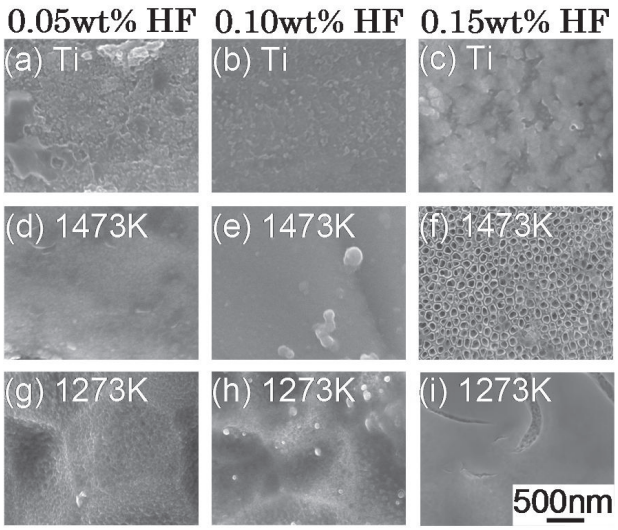

Fig. 7 SEM images of the specimens after anodic oxidation in the H_2SO_4-HF mixed solutions. (a) - (c): Sintered titanium specimens. (d) - (f): Lining layers produced at 1473 K. (g) - (i): Lining layers produced at 1273 K

In Fig. 7(f), a nanoporous oxide film was formed uniformly on the surface of the specimen heat-treated at 1473 K and anodized by using the solution of 1 kmol/m^3 H_2SO_4 with 0.15wt% HF. The average diameter and the depth of the pores were about 100 nm and 200 nm, respectively. On the other hand, no nanopore was formed in the other specimens. This reason is as follows.

In the case of the specimens from (a) to (e), the oxide did not dissolve enough to produce nanopores and thus formed barrier-type oxide films probably because sufficient F^- ion was not supplied. In the case of (g), (h) and (i), on the other hand, only the bottoms of the nanopores were observed on the surface, which are the vestige of excessive dissolution of the oxide.

From the results shown in Fig. 7, optimal condition for producing the nanoporous oxide film was detected for the planar lining layer.

Figure 8 presents SEM images of the inner wall of the microchannel after anodic oxidation performed under the optimal condition.

In this specimen, the nanoporous structure was observed near the both ends of the microchannel. However, it was not formed deep inside the microchannel. The nanopores seem to have been beginning to form but they are almost unfinished. This is probably because of insufficient electric charge. If so, nanoporous oxide film can be successfully produced by long-time anodic oxidation.

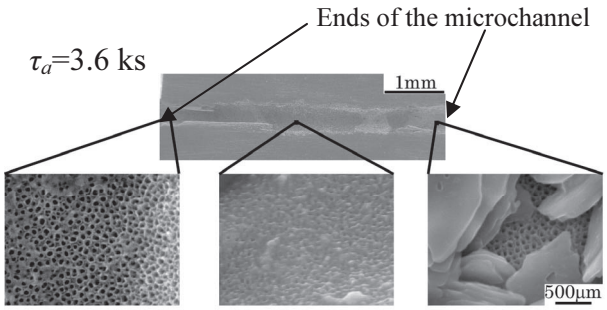

Fig. 8 SEM images of the inner wall of the microchannel produced at 1473 K and anodic-oxidized by using the solution of 1 kmol/m^3 H_2SO_4 with 0.15wt% HF

Figure 9 depicts the results of lengthening the anodic oxidation time. Mature nanoporous oxide film also produced deep inside the microchannel in each specimen.

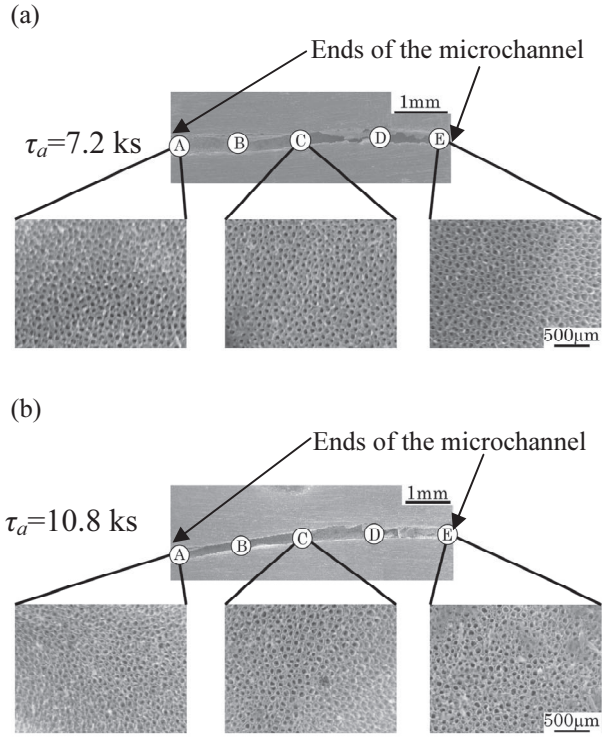

Fig. 9 SEM images of the inner wall of the microchannel produced at 1473 K and anodic-oxidized by using the solution of 1 kmol/m^3 H_2SO_4 with 0.15wt% HF and longer anodic-oxidation times, 7.2 ks (a) and 10.8 ks (b)

Figure 10 shows the average diameter, d_{np}, and the area number density, ρ_{np}, of the nanopores in the specimens shown in Fig. 9. The measurement locations, A to E, for each specimen were presented in Fig. 9.

In Fig. 10, neither d_{np} nor ρ_{np} was changed with the location and the anodic oxidation time.

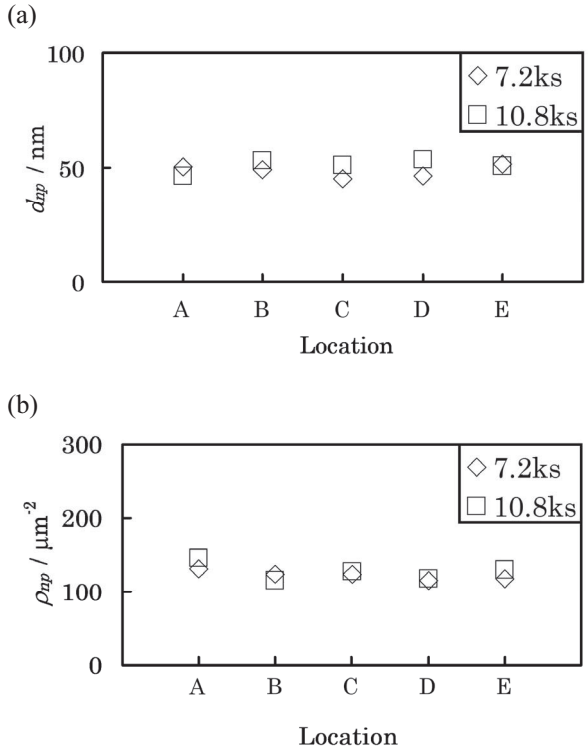

Fig. 10 Average diameter of nanopores, d_{np}, (a) and area number density of nanopores, ρ_{np}, (b)

4. Conclusions

Fabrication of the nanoporous oxide film on the inner walls of the microchannel and the plate-like cavity produced by Ti-Al reactive infiltration was examined. The results obtained are summarized as follows.

(1) The surface of the planar lining layer which was produced at 1473 K mainly consisted of titanium solid solution. The nanoporous oxide film was formed uniformly on the surface anodic oxidized for 3.6 ks in the solution of 1 kmol/m^3 H_2SO_4 with 0.15wt% HF. The average diameter and the depth of the pores were about 100 nm and 200 nm, respectively.

(2) Nanopores were formed near the exits of the microchannel but not deep inside the microchannel in the case of 3.6 ks anodic oxidation.

(3) The nanoporous oxide film was formed deep inside the microchannel by lengthening the anodic oxidation time.

(4) Almost uniform nanoporous oxide films covered the entire area of the inner wall of the microchannel when the anodic oxidation time was 7.2 ks or 10.8 ks.

References

[1] Ohmi, T., Sakurai, M., Matsuura, K. and Kudoh, M.: Formation of Microchannels in Sintered Titanium-Powder Compacts by Local Reactive Infiltration, *Proc. 15th Int. Symp. on Trans. Phenomena*, (2004), 364-367.

[2] Ohmi, T., Matsuura, K. Kudoh, M.: Formation of Intermetallic-Lined Microchannels in Sintered Metals by Local Reactive Infiltration, *Int. J. Self-Propagating High-Temperature Synthesis*, **13-2** (2004), 121-129.

[3] Ohmi, T., Takatoo, M., Iguchi, M., Matsuura, K. and Kudoh, M.: Powder-Metallurgical Process for Producing Metallic Microchannel Devices, *Mater. Trans.*, **47** (2006), 2137-2142.

[4] Ohmi, T., Sakurai, M., Matsuura, K., Kudoh, M. and Iguchi, M.: Formation of Microchannels in Sintered Titanium-Powder Compacts by Microscopic Reactive Infiltration, *I. J. Trans. Phenomena*, **9. 2** (2007), 105-111.

[5] Schuster, J. C. and Palm, M.: Reassessment of the Binary Aluminum-Titanium Phase Diagram, *JPEDAV*, **27** (2006), 255-277

[6] Tsuchiya, H., Berger, S., Macak, J. M., Ghicov, A., Schmuki, P.: Self-Organized Porous and Tubular Oxide Layers on TiAl Alloys, *Electrochemistry Communications*, **9** (2007), 2397–2402.

[7] Jennings, J. R., Ghicov, A., Peter, L. M., Schmuki, P., and Walker, A. B.: Dye-Sensitized Solar Cells Based on Oriented TiO_2 Nanotube Arrays: Transport, Trapping, and Transfer of Electrons, *J. Am. Chem. Soc.*, **130** (2008), 13364-13372.

[8] Yasuda, K. and Schmuki, P.: Control of Morphology and Composition of Self-Organized Zirconium Titanate Nanotubes Formed in $(NH_4)_2SO_4/NH_4F$ Electrolytes, *Electrochimica Acta*, **52** (2007), 4053–4061.

[9] Macak, J. M., Tsuchiya, H., and Schmuki, P: High-Aspect-Ratio TiO_2 Nanotubes by Anodization of Titanium, *Angew. Chem. Int. Ed.*, **44** (2005), 2100 – 2102.

[10] Taveira, L. V., Macak, J. M., Tsuchiya, H., Dick, L. F. P., and Schmuki, P.: Initiation and Growth of Self-Organized TiO_2 Nanotubes Anodically Formed in $NH_4F/(NH_4)_2SO_4$ Electrolytes, *Journal of The Electrochemical Society*, **152** (2005), B405-B410.

[11] Yasuda, K., Macak, J. M., Berger, S., Ghicov, A., and Schmuki, P. Mechanistic Aspects of the Self-Organization Process for Oxide Nanotube Formation on Valve Metals, *Journal of The Electrochemical Society*, **154** (2007), C472-C478.